Ethylene Epoxidation with Tungsten Diperoxo Complexes: Is Relativity the Origin of Reactivity?

Dirk V. Deubel

Department of Chemistry, University of Calgary, Calgary, Alberta, Canada T2N 1N4

Received: January 4, 2001; In Final Form: February 28, 2001

Scalar-relativistic effects on the coarctate transition states (TS) for ethylene epoxidation with Mimoun-type diperoxo complexes [$MO(\eta^2\text{-}O_2)_2(OPH_3)$], M = Cr, Mo, W, were studied using gradient-corrected density-functional theory at the BP86 level within the nonrelativistic, quasi-relativistic, and ZORA approaches. Spin−orbit effects were proved to be small. While scalar-relativistic effects scarcely influence the thermodynamics of the reaction with the tungsten complex, they shift the extent of reaction at the transition state toward the reactants and decrease the activation barrier significantly. The analysis of the transition states using a fragment-based energy-decomposition scheme shows that the reduction of the activation energy by relativistic effects is mainly due to the destabilization of the reactants rather than to the stabilization of the TS.

Introduction

The development of efficient processes for the oxidation of olefins on a million-ton-per-year scale remains an important goal in the chemical industry.[1] Recently, a method for alkene epoxidation using Mimoun-type diperoxo complexes[2] [$MoO(O_2)_2(OPR_3)$] (R = alkyl) as catalysts[3] in a biphasic system was introduced by Sundermeyer and co-workers[4] and patented by BASF.[5] Several theoretical studies on the epoxidation of olefins with peroxo complexes of groups 6 and 7 were reported.[6−11] After a long-standing controversy,[12] the reaction mechanism of olefin epoxidation with diperoxo complexes of type [$MoO(O_2)_2(OPR_3)$] was recently clarified with the help of density-functional methods. As suggested by Sharpless and co-workers,[13] the reaction follows a concerted oxygen-transfer mechanism.[8b] The oxygen atom trans to the phosphine oxide is transferred;[8b] Figure 1 shows the optimized structure of the transition state (TS). The topology of the TS is coarctate.[14]

Recent density-functional-theory (DFT) calculations on the control of reactivity of olefin epoxidation with diperoxo complexes revealed that the corresponding tungsten compound reacts faster than the parent molybdenum complex.[8e] This result is in agreement with a recent theoretical study by Rösch and co-workers[7c] on ethylene epoxidation with other diperoxo complexes of group 6. However, little is known about the reason for the increased reactivity of the third-row transition-metal complexes. It would be particularly interesting to learn the role that relativistic effects play. In former DFT studies on olefin epoxidation with diperoxo complexes,[6−8] a pseudo-relativistic effective-core potential (ECP) was employed for the metal.[17] It has not yet been clarified whether the lower activation energy of the tungsten complex is due to relativity. This information can only be obtained by comparing the results of relativistic and nonrelativistic calculations.

The objective of this comparative density-functional study is to elucidate relativistic effects on the transition-state geometries and activation energies for ethylene epoxidation by [$MO(\eta^2\text{-}O_2)_2(OPH_3)$] with M = Cr, Mo, W. The transition states at the BP86 level within the nonrelativistic approach (NR), the quasi-relativistic approach (QR), and the zeroth-order regular approximation (ZORA) have been calculated and analyzed using the Extended Transition State (ETS) method, which was developed by Ziegler and Rauk.[18,19] With this energy-decomposition scheme,[18] we are able to describe the TSs in terms of interactions between the fragments ethylene and diperoxo complex in order to gain insight into the origin of reactivity.

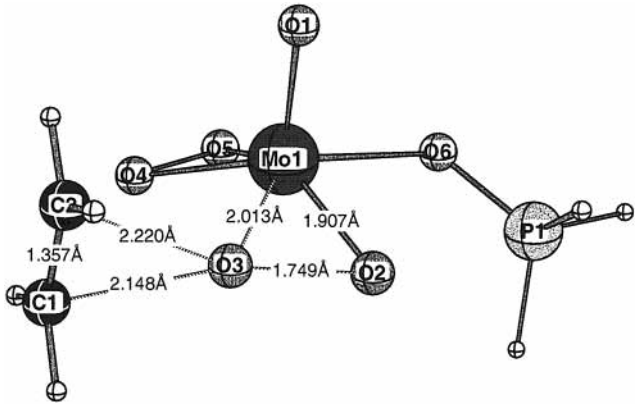

Figure 1. Calculated transition structure (BP86/ZORA/III~) for ethylene epoxidation with [$MoO(O_2)_2(OPH_3)$]. Selected bond angles (deg): Mo−O2−O3 66.7; Mo−O3−O2 60.4; O2−Mo−O3 52.9; C1−C2−O3 69.0; C2−C1−O3 74.8; C1−O3−C2 36.1.

Methods

Density-Functional Calculations. Molecules and transition states were optimized at the gradient-corrected density-functional-theory (DFT) level using the exchange functional of Becke[20] and the correlation functional of Perdew[21] (BP86). Uncontracted Slater-type orbitals (STOs) were used as basis functions for the SCF calculations.[22] The basis functions at the metals have triple-ζ quality, augmented with a set of p functions. The basis set at the other atoms has double-ζ quality, augmented with a set of d-type polarization functions. The $(1s)^2$ core electrons of C, N, and O, the $(1s2s2p)^{10}$ core electrons of P and Cr, the $(1s2s2p3s3p3d)^{28}$ core electrons of Mo, and the $(1s2s2p3s3p3d4s4p4d)^{46}$ core electrons of W were treated within the frozen-core approximation.[23] An auxiliary basis set of s, p, d, f, and g STOs was utilized to fit the molecular densities and

10.1021/jp0100497 CCC: $20.00
Published on Web 04/24/2001

to represent the Coulomb and exchange potentials in each SCF cycle.[24] This basis-set combination is denoted III∼.[25] Improved total energies were calculated using triple-ζ quality basis sets, augmented with a set of p and f functions at the metal and augmented with a set of d and f functions at the other atoms. As with the previously discussed basis set, the inner shells of the atoms were frozen. This basis-set combination is denoted V. The calculations were carried out with the ADF 2000 program package.[26] The results were compared to results at the BP86 and B3LYP[27] levels using basis sets II[28] and III+[29] with a small-core effective potential (ECP)[17] at the metal. Basis set II consists of this ECP, together with a {441/2111/*n*1} ($n = 4$ (Cr), $n = 3$ (Mo), $n = 2$ (W)) valence-basis set at the metal and 6-31G(d) all-electron basis sets at the other atoms.[30] Basis set III+ uses the same ECP and valence-basis set at the metals, but totally uncontracted and augmented with one set of f-type polarization functions,[31] together with 6-31+G(d) basis sets at the other atoms.[32] Vibrational frequencies of the Mo compounds were calculated at the B3LYP/II level in a former study to validate the stationary points.[8b] Starting with the TS geometries, calculations of the Intrinsic Reaction Coordinate (IRC)[33] were carried out in order to find out the respective reactants and products.[8b] All calculations with the basis sets II and III+ including the ECP were performed using the Gaussian 98 package.[34]

Consideration of Relativistic Effects.[35] Evaluating the time-independent Dirac equation:[36]

$$(c\alpha p + \beta mc^2 + V)\psi = E\psi \tag{1}$$

in 2 × 2-block-diagonal form,[37] gives the relation between the small component ψ_S and the large component ψ_L of the Dirac spinor ψ as the starting point of the first-order method (FO)[38] and the zeroth-order regular approximation (ZORA):[39]

$$\psi_S = (2mc^2 + E - V)^{-1}\, c\sigma p\psi_L = \lambda\, c\sigma p\psi_L \tag{2}$$

Factoring out $(2mc^2)^{-1}$ and expanding in first order leads to the FO approach:

$$\lambda_{FO} = (2mc^2)^{-1}\left(1 + \frac{E-V}{2mc^2}\right)^{-1} \approx (2mc^2)^{-1}\left(1 - \frac{E-V}{2mc^2}\right) \tag{3}$$

and to the Pauli equation:

$$\left(\frac{p^2}{2m} + V + \frac{Zs(r\times p)}{2m^2c^2r^3} - \frac{p^4}{8m^3c^2} + \frac{Z\pi\delta(r)}{2m^2c^2}\right)\psi_L = E\psi_L \tag{4}$$

with the Schrödinger Hamiltonian ($p^2/2m + V$) and the spin−orbit, mass−velocity, and Darwin corrections. The latter two terms are denoted scalar-relativistic corrections. The first-order results can significantly be improved by a quasi-relativistic approach (QR)[40] where energy corrections consider relativistic changes in electron density.[40c] However, in the case of the singular Coulomb potential, the expansion in $(E - V)/2mc^2$ diverges near the nucleus.[39f] Therefore, we have also performed calculations using the reliable zeroth-order regular approximation (ZORA),[39] which is obtained from eq 2 by factoring out $(2mc^2 - V)^{-1}$ and expanding in zeroth order:

$$\lambda_{ZORA} = (2mc^2 - V)^{-1}\left(1 + \frac{E}{2mc^2 - V}\right)^{-1} \approx (2mc^2 - V)^{-1} \tag{5}$$

In the present work, the scalar-relativistic QR and ZORA methods have been utilized and the results were compared to the results of nonrelativistic (NR) calculations. Spin−orbit effects on selected molecules and transition states have been considered by ZORA energy calculations using the scalar-relativistic geometries. Unless otherwise mentioned, "relativistic corrections" refer to the differences between the NR and scalar-relativistic ZORA results at the BP86/III∼ level.

Energy Decomposition in the Transition States. Energy decomposition in the TSs was examined using the Extended Transition State (ETS) method developed by Ziegler and Rauk.[18] The TSs are divided into the fragments ethylene and diperoxo complex. The activation energy ΔE is partitioned into the two contributions strain energy ΔE_{str} and interaction energy ΔE_{int}:

$$\Delta E = \Delta E_{str} + \Delta E_{int} \tag{6}$$

The strain energy ΔE_{str} is the difference between the energy of the isolated fragments in the TS geometry and their energy in the equilibrium geometry. ΔE_{int} represents the energy of interaction between the isolated fragments in the TS geometry and can in turn be partitioned into three components:

$$\Delta E_{int} = \Delta E_{elst} + \Delta E_{Pauli} + \Delta E_{orb} \tag{7}$$

ΔE_{elst} gives the electrostatic interaction energy between the fragments, which is calculated with a frozen electron-density distribution in the TS geometry. ΔE_{Pauli} is the repulsive interaction energy between the fragments that is caused by the fact that two electrons with the same spin cannot occupy the same region in space. ΔE_{Pauli} is calculated by enforcing the Kohn−Sham determinant which is the result of the two superimposing fragments ethylene and diperoxo complex to obey the Pauli principle through antisymmetrization and renormalization. Finally, the orbital-interaction term ΔE_{orb} is calculated with the Kohn−Sham orbitals relaxing to their optimal form.

Results and Discussion

Transition-State Geometries and Activation Energies. Former theoretical studies[7cd,8] on Mo-catalyzed epoxidations were carried out using the 3-parameter-Hartree−Fock-DFT hybrid functional (B3LYP) and basis set II[28] or a similar basis set with the same small-core ECP at the metal.[17] We briefly compare these results to new results obtained by calculations using the BP86 functional within the ZORA approach (BP86/ZORA/III∼). Figure 1 shows the theoretically predicted geometry of the transition state for ethylene epoxidation with $[MoO(\eta^2\text{-}O_2)_2(OPH_3)]$;[41] Table 1 lists selected geometrical parameters and the activation energy ΔE at several DFT levels. It is interesting to note that there is a significant difference in the activation barriers calculated at the B3LYP/II (13.8 kcal/mol)[8b] and BP86/ZORA/III∼ levels (6.1 kcal/mol). The value obtained at the BP86/II level (6.6 kcal/mol) clearly demonstrates that this energy difference arises from the functional rather than from the effective-core potential. Since activation barriers are underestimated by DFT[42] and the use of the model ligand $OPMe_3$ instead of OPH_3 gives systematic activation-energy corrections of 2.5 kcal/mol,[8b] the present work should be considered a contribution toward a qualitative understanding of relativistic effects on reactivity rather than a report of quantitative data. The employment of improved basis sets for geometry optimization leads to considerable changes in absolute interatomic distances of up to 0.05 Å but to small changes in activation energies (Table 1).

In this section, we compare the nonrelativistic and relativistic calculations for ethylene epoxidation with the three peroxo

TABLE 1: Selected Bond Distances (Å) in the Transition States (TS), Reactants, and Products of Ethylene Epoxidation with Mimoun-Type Diperoxo Complexes [$MoO(O_2)_2(OPH_3)$], the Extent of Reaction ξ(TS) at the TSs, Activation Energies ΔE, and Reaction Energies ΔE_r (kcal/mol)

	TS						reactant[a]			prod.[b]			
method	M−O2	M−O3	O2−O3	C1−O3	C2−O3	C1−C2	M−O2	M−O3	O2−O3	M−O2	ξ(TS)	ΔE	ΔE_r
B3LYP/II	1.870	2.015	1.789	2.078	2.186	1.360	1.932	1.947	1.451	1.722	0.274	13.8	−34.7
B3LYP/III+	1.852	2.005	1.786	2.115	2.179	1.361	1.915	1.929	1.456	1.703	0.267	14.2	−37.2
BP86/II	1.903	2.005	1.738	2.129	2.273	1.367	1.943	1.956	1.465	1.737	0.214	6.6	−32.5
BP86/III+	1.888	1.995	1.740	2.165	2.258	1.368	1.926	1.940	1.471	1.719	0.213	7.0	−35.1
BP86/ZORA/III∼	1.907	2.013	1.749	2.148	2.220	1.357	1.973	1.966	1.475	1.732	0.221	6.1	−31.9
BP86/ZORA/V	1.890	1.991	1.748	2.152	2.240	1.357	1.920	1.931	1.471	1.719	0.221	8.2	−32.3

[a] Ethylene: C−C: 1.331 (B3LYP/II), 1.335 (B3LYP/III+), 1.340 (BP86/II), 1.344 (BP86/III+), 1.332 (BP86/ZORA/III∼), 1.333 (BP86/ZORA/V). [b] Oxirane: C−O, C−C: 1.440, 1.477 (B3LYP/II), 1.444, 1.478 (B3LYP/III+), 1.429, 1.469 (BP86/II), 1.434, 1.470 (BP86/III+), 1.442, 1.467 (BP86/ZORA/III∼), 1.440, 1.470 (BP86/ZORA/V).

TABLE 2: Calculated (BP86/III∼) Bond Distances (Å) in the Transition States (TS), Reactants, and Products of Ethylene Epoxidation with Mimoun-Type Diperoxo Complexes [$MO(O_2)_2(OPH_3)$], M = Cr, Mo, W, the Extent of Reaction ξ(TS) at the Transition States, Activation Energies ΔE, and Reaction Energies ΔE_r (kcal/mol)

		TS						reactant[a]			prod.[b]			
M	method	M−O2	M−O3	O2−O3	C1−O3	C2−O3	C1−C2	M−O2	M−O3	O2−O3	M−O2	ξ(TS)	ΔE	ΔE_r
Cr	NR	1.755	1.926	1.713	2.188	2.112	1.359	1.805	1.849	1.428	1.602	0.242	9.1	−37.2
	QR	1.753	1.921	1.712	2.189	2.121	1.358	1.802	1.844	1.432	1.600	0.236	8.6	−37.5
	ZORA	1.753	1.921	1.712	2.189	2.121	1.358	1.802	1.844	1.432	1.600	0.236	8.6	−37.7
Mo	NR	1.912	2.025	1.753	2.119	2.219	1.358	1.979	1.976	1.468	1.739	0.235	7.2	−31.6
	QR	1.909	2.011	1.752	2.134	2.234	1.357	1.974	1.963	1.478	1.734	0.220	6.1	−31.8
	ZORA	1.907	2.013	1.749	2.148	2.220	1.357	1.973	1.966	1.475	1.732	0.221	6.1	−31.9
W	NR	1.933	2.037	1.758	2.152	2.220	1.357	1.999	1.992	1.478	1.763	0.228	6.5	−30.8
	QR	1.916	1.987	1.749	2.184	2.294	1.354	1.977	1.950	1.502	1.736	0.194	3.3	−31.9
	ZORA	1.915	1.988	1.752	2.200	2.280	1.354	1.975	1.950	1.501	1.739	0.194	3.9[c]	−31.8[c]

[a] Ethylene (NR, QR, and ZORA): C−C 1.332. [b] Oxirane (NR, QR, and ZORA): C−O 1.442, C−C 1.467. [c] Including spin−orbit effects: ΔE = 3.8 kcal/mol, ΔE_r = −31.8 kcal/mol.

complexes [$MO(\eta^2\text{-}O_2)_2(OPH_3)$]. Selected structural parameters of the TSs, the reactants, and the products as well as theoretically predicted activation energies with the three metals Cr, Mo, and W at the NR level and at the scalar-relativistic QR and ZORA levels are listed in Table 2. The calculations reveal that the QR and ZORA results are very similar: The largest differences in interatomic distances and relative energies are 0.016 Å and 0.6 kcal/mol, respectively. In addition, we have considered spin−orbit effects on the activation and reaction energy although the net first-order effect is zero in closed-shell systems, such as the present molecules. Spin−orbit calculations using the scalar-relativistic ZORA geometries of the tungsten compounds show that the corrections in the activation and reaction energy are less than 0.1 kcal/mol (Table 2). In the discussion of relativity in the following paragraphs, we refer to the differences between the nonrelativistic and scalar-relativistic ZORA results at the BP86/III∼ level.

Olefin epoxidation by diperoxo compounds of group 6 with ammine ligands was recently studied by Rösch and co-workers, using an ECP at the metal.[7c] They predict a reduction of the activation barriers in the order Cr > Mo > W.[7c] The results of the current work on ethylene epoxidation with [$MO(\eta^2\text{-}O_2)_2(OPH_3)$] at the ZORA level confirm this trend (Table 2): The activation energies ΔE of the "real" molecules, i.e., investigated at the ZORA level, are 8.6 (Cr), 6.1 (Mo), and 3.9 (W) kcal/mol. The major contribution to the decrease of the activation barrier arises from relativity: The nonrelativistic activation energies are higher by 0.5 (Cr), 1.1 (Mo), and 2.6 (W) kcal/mol. In contrast to the activation barriers, the differences between the reaction energies ΔE_r for the olefin epoxidations on the NR and ZORA potential-energy surfaces are rather small, at most 1 kcal/mol (Table 2). Surprisingly, the reaction with the Cr compound has the largest thermodynamic driving force but the highest barrier, i.e., the Bell−Evans−Polanyi principle[43] is useless to predict qualitative changes in reactivity. The Hammond postulate[44] also fails; despite a larger thermodynamic driving force, the reaction with the chromium complex proceeds via a later TS: Selected structural parameters of the reactants, transition states, and products are also given in Table 2. We focus on the extent of reaction $\xi(TS)$ in the transition state, which we define in a straightforward way (eq 8 where the a and b values refer to the distances in the reactants (re), TSs, and products (pr) shown in Scheme 1):

$$\xi(\mathrm{TS}) = \frac{a(\mathrm{TS}) - a(re)}{a(\mathrm{TS}) - a(re) + b(TS) - b(\mathrm{pr})} \qquad (8)$$

The calculations reveal that the extent of reaction is shifted toward the reactants due to relativistic effects (Table 2). The largest energy difference of ξ(TS) between the values in the NR (0.23) and ZORA (0.19) approaches is found for the tungsten compound. We would like to point out a remarkable correlation between the activation energy ΔE and the extent of reaction $\xi(TS)$: The earlier the transition state on the reaction coordinate, the higher is the reactivity of the complex (Figure 2).[45]

Although the relation between the extent of reaction and the activation barrier is interesting, a prediction of the reactivity based on properties of the *reactants* rather than of the *transition states* would be of a larger practical use. In a very recent study on ethylene epoxidation with several oxidants,[8c] we showed that the predominant orbital interaction between the oxidant and the olefin in the transition state is the interaction between the olefin HOMO and the σ^* orbital of the O−O bond that is cleaved (Scheme 2).[46] Rösch and co-workers[7c] recently investigated other diperoxo complexes of group 6 and pointed out that there is a correlation between the σ^*-orbital energy ϵ and the activation barrier ΔE: The lower this orbital energy, the higher

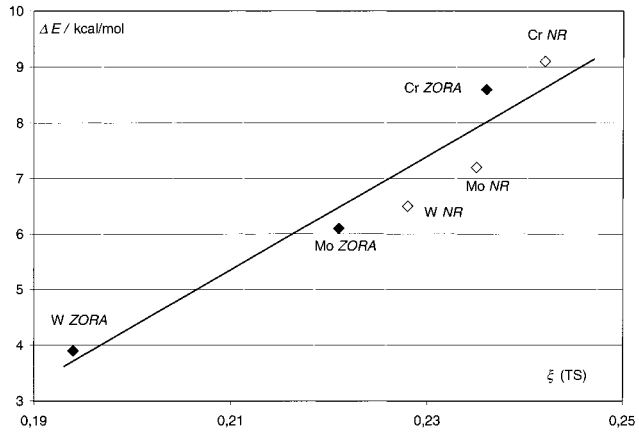

Figure 2. Correlation of the activation energies ΔE to the extent of reaction ξ(TS) in the transition states.

SCHEME 1: On the Definition of the Extent of Reaction ξ(TS) in the Transition States for Olefin Epoxidation with Mimoun-Type Diperoxo Complexes

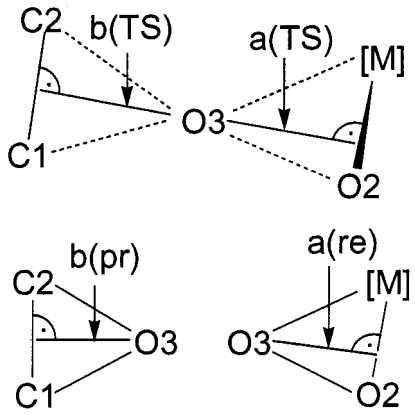

SCHEME 2: Predominant Orbital Interactions in the Transition States for Olefin Epoxidation with Mimoun-Type Diperoxo Complexes

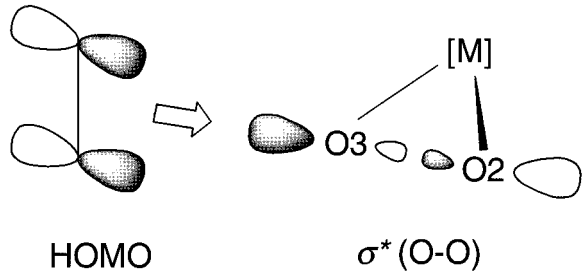

is reactivity. We are not going to repeat similar results here but it should be pointed out that the calculations on complexes of type $[MO(\eta^2\text{-}O_2)_2(OPH_3)]$ seem to support these ideas very well, both at the nonrelativistic and relativistic levels (Figure 3).

Fragment Analysis of the Transition States. To gain insight into the origin of the activation energy, the transition states for olefin epoxidation have been analyzed in terms of interactions between the fragments ethylene and diperoxo complex. This approximation is justified because the reactions have early transition states with ξ(TS) values between 0.19 and 0.25 (Table 2). Prior to the analysis of all TSs, we would like to demonstrate how the interactions between the two fragments proceed during the reaction. Ethylene epoxidation with the tungsten complex $[WO(\eta^2\text{-}O_2)_2(OPH_3)]$ at the ZORA level was chosen as example. We have analyzed the energy decomposition at points on the potential-energy surface before (TS−), at (TS), and after (TS+)

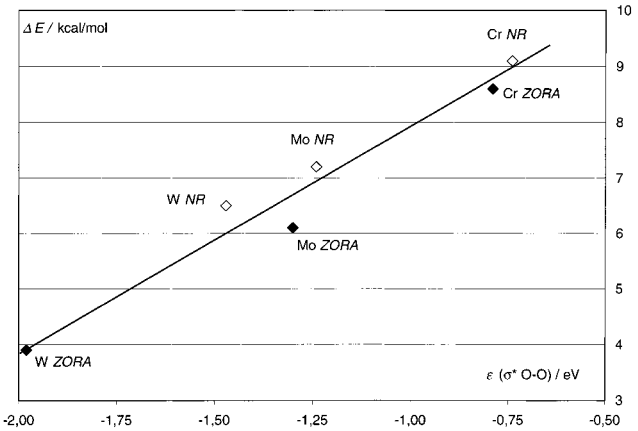

Figure 3. Correlation of the activation energies ΔE to the σ*(O−O)-orbital-energy level ϵ of the O−O bond in the reactant.

TABLE 3: Fragment Analysis of Selected Points along the Reaction Coordinate[a] before (TS−), at (TS), and after (TS+) the Transition State for Ethylene Epoxidation with $[WO(O_2)_2(OPH_3)]$, at the BP86/ZORA/III∼ Level (energies in kcal/mol)

	ΔE_{str} ($[M]O_2$)	ΔE_{str} (ethylene)	ΔE_{str} (total)	ΔE_{Pauli}	ΔE_{elst}	ΔE_{ort}	ΔE_{int}	ΔE
TS−	6.6	0.1	6.7	46.9	−25.3	−27.4	−3.1	3.6
TS	11.4	0.4	11.8	60.0	−31.6	−36.2	−7.8	3.9
TS+	16.8	0.7	17.5	77.5	−39.7	−51.9	−14.1	3.4

[a] The geometries of TS− and TS+ were calculated by adding −0.1 and 0.1, respectively, of the eigenvector that corresponds to the negative eigenvalue of the force-constants matrix to the coordinates of the stationary point.

the transition state.[47] The energy contributions are listed in Table 3 and visualized in Figure 4. We start with the reactants approaching each other from an infinite distance, where all energy contributions are zero. Pauli repulsion (ΔE_{Pauli}), which steadily increases during the reaction, considers the energy required for antisymmetrization and re-normalization of the Kohn−Sham orbitals of the superimposing fragments ethylene and diperoxo complex. This repulsive term is overcompensated by the two stabilizing terms electrostatics (ΔE_{elst}) and orbital interactions (ΔE_{orb}). The sum of these three contributions result in a net stabilizing interaction energy (ΔE_{int}), which also increases along the reaction coordinate. Before the fragments can interact, however, the two isolated fragments have to be deformed out of their equilibrium geometry; the energy required is the so-called strain energy (ΔE_{str}). The contribution from the ethylene deformation (ΔE_{str}(ethylene)) is negligible, while the deformation of the diperoxo complex $[M]O_2$ causes the major contribution to ΔE_{str}. The strain energy is larger than the stabilization by the interaction ΔE_{int}, yielding positive ΔE values at the investigated points. At the TS, ΔE reaches a maximum and is identical to the activation barrier (Figure 4b).

The correlation between the energy level of the σ* orbital and the activation energy, which has been pointed out in the former section, suggests that the orbital interactions in the TS for the tungsten complexes at the relativistic levels are strongest and cause the higher reactivity. To support this simple hypothesis, the transition states for ethylene epoxidation with the three metal complexes have been investigated at the nonrelativistic and relativistic levels. The results are given in Table 4 and Figure 5. The analysis shows a significant decrease of Pauli repulsion within the triad Cr/Mo/W, which is mainly caused by relativity (Figure 5a). There are again the stabilizing terms ΔE_{elst} and ΔE_{orb}. The latter contribution is particularly interesting: One might expect that the stabilization of the transition

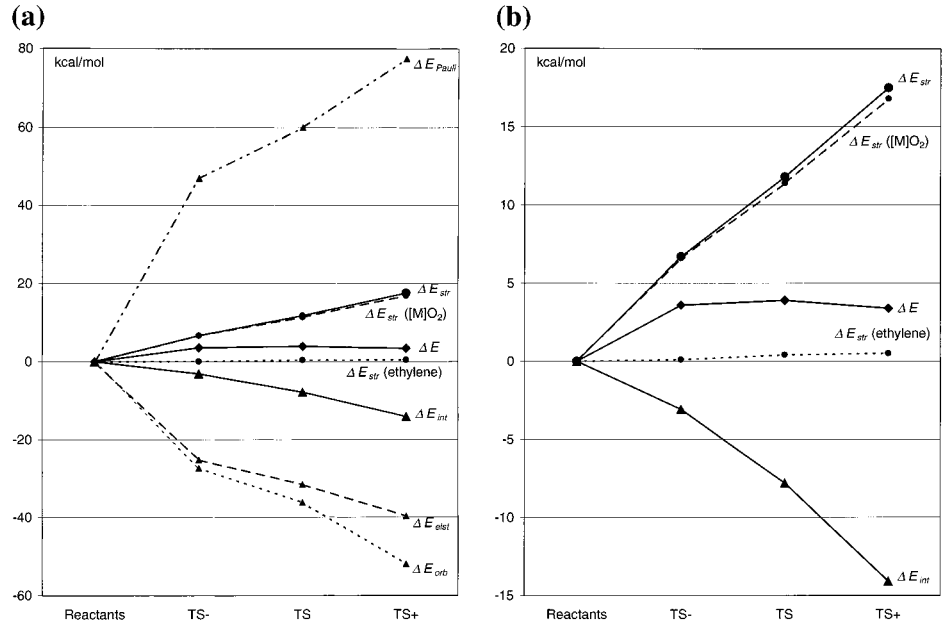

Figure 4. Fragment analysis at selected points before (TS−), at (TS), and after (TS+) the transition state for ethylene epoxidation with [WO-$(O_2)_2(OPH_3)$], calculated at the BP86/ZORA/III∼ level.

TABLE 4: Fragment Analysis of the Transition States at the BP86/III∼ Level (energies in kcal/mol)

M	method	ΔE_{str} ([M]O_2)	ΔE_{str} (ethylene)	ΔE_{str} (total)	ΔE_{Pauli}	ΔE_{elst}	ΔE_{ort}	ΔE_{int}	ΔE
Cr	NR	16.4	0.5	16.9	76.6	−38.8	−45.6	−7.8	9.1
	QR	15.7	0.5	16.2	75.4	−38.2	−44.8	−7.6	8.6
	ZORA	15.7	0.5	16.2	75.4	−38.2	−44.8	−7.6	8.6
Mo	NR	15.2	0.5	15.7	73.5	−37.5	−44.6	−8.6	7.2
	QR	14.1	0.5	14.6	70.3	−36.2	−42.7	−8.5	6.1
	ZORA	14.0	0.5	14.5	69.6	−35.7	−42.3	−8.4	6.1
W	NR	14.4	0.5	14.9	69.8	−36.2	−42.1	−8.5	6.5
	QR	11.3	0.4	11.7	61.1	−33.6	−36.9	−8.4	3.3
	ZORA	11.4	0.4	11.8	60.0	−31.6	−36.2	−7.8	3.9

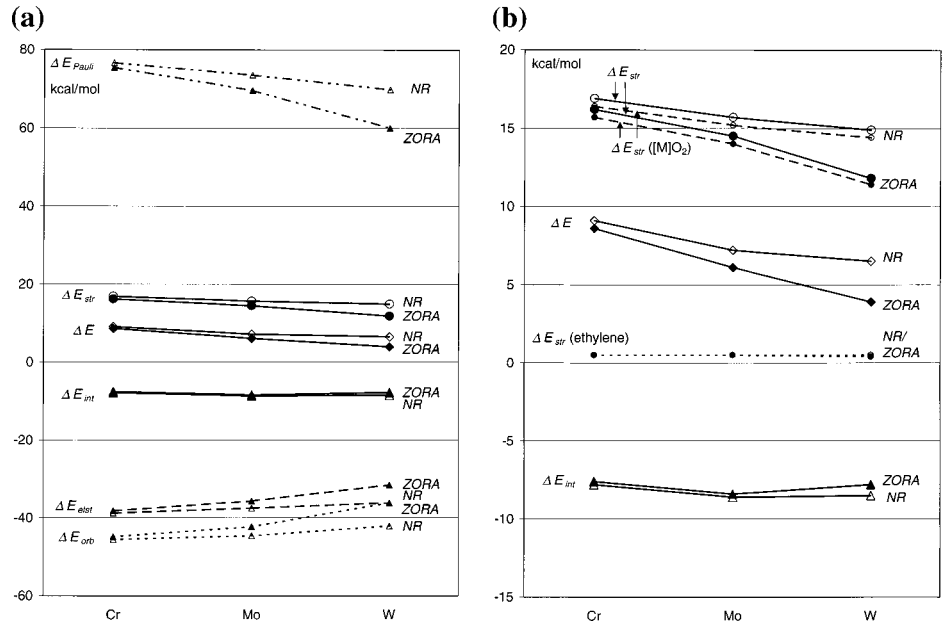

Figure 5. Fragment analysis of the transition states for ethylene epoxidation with $[MO(O_2)_2(OPH_3)]$, (M = Cr, Mo, W), calculated at the BP86/III∼ level within the NR and ZORA approaches.

states by orbital interactions is largest for the tungsten compound at the relativistic levels because the σ^* orbital is lowest in energy (Figure 3). However, the opposite is the case: The stabilizing orbital-interaction energy is smallest in the TS for the most reactive compound. We find that weaker orbital interactions together with smaller electrostatic stabilization in the TS are compensated by the reduction of Pauli repulsion, making the interaction energy be almost equal in all investigated transition states, both at the nonrelativistic and relativistic levels (Table 4, Figure 5b). The interaction between ethylene and the diperoxo

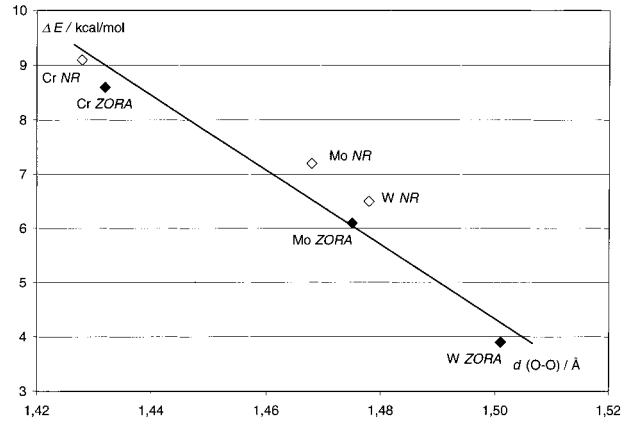

Figure 6. Correlation of the activation energies ΔE to the O−O bond distance d in the reactant.

complex in the transition state does therefore not control the reactivity. In contrast, the activation energies ΔE are completely reflected by the total strain energies ΔE_{str} and particularly by the strain energies of the metal fragment $\Delta E_{str}([M]O_2)$ (Figure 5b). Therefore, the origin of the low activation barrier for the tungsten complex is simply a smaller deformation out of the equilibrium structure toward the transtion-state geometry. Consider again the geometries of the reactants and transition states given in Table 2: The most significant change is found for the O−O distances in the reactants. Relativistic effects elongate these bonds particularly in the tungsten complex. Certainly, all W−O bonds in the reactants, TSs, and products are contracted by relativistic effects. Due to the mass-velocity contribution, the reduction of kinetic energy is smaller when bonds become shorter.[35,48] Since tungsten forms stronger bonds to the oxygen atoms of the peroxo functionality, the remaining O−O bond of the metalladioxirane moiety (WO_2) is weakened.

We would like to point out that the correlation between the activation energy ΔE with the σ*-orbital energy levels is no contradiction to the results of the fragment analysis, although Figure 3 is misleading: Low energies of the σ* orbital are not the reason for a higher reactivity. They are just a measure for the strengh of the O−O bond of the peroxo ligand since, in weaker bonds, there is a smaller energy gap between the bonding and antibonding orbitals. Another measure of the O2−O3 bond strength is simply the interatomic distance. We demonstrate in Figure 6 that a prediction of the activation energy by the oxygen−oxygen distances of the reactants is possible for diperoxo complexes of type $[MO(\eta^2\text{-}O_2)_2(OPH_3)]$. This is a very interesting result because a theoretical study[15h] on the epoxidation of olefins and other substrates with several oxidants revealed that the large differences in the reactants' O−O bond energies do not necessarily imply that the activation barriers must differ from each other. For olefin epoxidation with the three model complexes investigated at relativistic and nonrelativistic levels, however, we find a remarkable relation of reactivity to parameters of the O−O bond such as bond length, orbital energies, and activation strain.

Conclusions

Scalar-relativistic corrections shift the extent of reaction ξ at the TS for ethylene epoxidation with group-6 diperoxo complexes $[MO(O_2)_2(OPH_3)]$ toward the reactants and decrease the activation energy. The metal−O(peroxo) bonds in the reactants are contracted and stabilized due to relativity, thus elongating and destabilizing the remaining O−O bond of the metalladioxirane moiety. The effects are certainly largest in the tungsten complex and smallest, but noticeable, in the chromium complex. The established concept of the interaction between the olefin HOMO and the σ* orbital of the O−O bond as the spearhead of reactivity has been scrutinized: In a recent study, a *correlation* of the σ*-orbital energy level with the activation energies was reported, i.e., the diperoxo complex with the lowest energy of the σ*-(O−O) orbital reacts fastest. However, the energy-decomposition analysis of the transition states reveals that the orbital-interaction energy is smallest in the TS for the most reactive oxidant. Low energies of the σ*-(O−O) orbital are not the *origin* of reactivity. They are simply a *measure* for the weakness of the O−O bond of the peroxo ligand: in weaker bonds, there is a smaller energy gap between the bonding and antibonding orbitals.

Acknowledgment. The author thanks Dr. Michael Seth, University of Calgary, and Dr. F. Matthias Bickelhaupt, Vrije Universiteit Amsterdam, for helpful discussions. He also thanks Prof. Dr. Tom Ziegler, Prof. Dr. Gernot Frenking, the Deutscher Akademischer Austauschdienst (NATO fellowship), and the Fonds der Chemischen Industrie (Kekulé scholarship) for financial support.

References and Notes

(1) (a) Wittcoff, H. A.; Reuben, B. G. *Industrial Organic Chemicals*; Wiley: New York, 1996. (b) Weissermel, K.; Arpe, H.-J. *Industrial Organic Chemistry*, 3rd ed.; Wiley-VCH: Weinheim, 1997.

(2) (a) Mimoun, H.; Seree de Roch, I.; Sajus, L. *Bull. Soc. Chem. Fr.* **1969**, 1481. (b) Mimoun, H.; Seree de Roch, I.; Sajus, L. *Tetrahedron* **1970**, *26*, 37. (c) Mimoun, H. *Angew. Chem.* **1982**, *94*, 750; *Angew. Chem., Int. Ed. Engl.* **1982**, *21*, 734.

(3) Note that, in the catalytic reaction, the complex $[MoO(\eta^2\text{-}O_2)_2(OPR_3)]$ is only one of the active species. For instance, protonated diperoxo species, which might exist in the catalytic system in small concentrations, are more reactive than the parent complex (ref 8d).

(4) Wahl, G.; Kleinhenz, D.; Schorm, A.; Sundermeyer, J.; Stowasser, R.; Rummey, C.; Bringmann, G.; Fickert, C.; Kiefer, W. *Chem. Eur. J.* **1999**, *5*, 3237.

(5) (a) Schulz, M.; Teles, J. H.; Sundermeyer, J.; Wahl, G. (BASF AG) *DE 195.33.331.4*, **1995**. (b) Schulz, M.; Teles, J. H.; Sundermeyer, J.; Wahl, G. (BASF AG) *WO 10054*, **1995**.

(6) Wu, Y. D.; Sun, J. *J. Org. Chem.* **1998**, *63*, 1752.

(7) (a) Gisdakis, P.; Antonczak, S.; Köstlmeier, S.; Herrmann, W. A.; Rösch, N. *Angew. Chem.* **1998**, *110*, 2333; *Angew. Chem., Int. Ed. Engl.* **1998**, *37*, 2211. (b) Kühn, F. E.; Santos, A. M.; Roesky, P. W.; Herdtweck, E.; Scherer, S.; Gisdakis, P.; Yudanov, I. V.; Di Valentin, C.; Rösch, N. *Chem. Eur. J.* **1999**, *5*, 3603. (c) Di Valentin, C.; Gisdakis, P.; Yudanov, I. V.; Rösch, N. *J. Org. Chem.* **2000**, *65*, 2996. (d) Yudanov, I. V.; Di Valentin, C.; Gisdakis, P.; Rösch, N. *J. Mol. Catal.* **2000**, *158*, 189. (e) Di Valentin, C.; Gandolfi, R.; Gisdakis, P.; Rösch, N. *J. Am. Chem. Soc.* **2001**, *123*, 2365.

(8) (a) Deubel, D. V.; Sundermeyer, J.; Frenking, G. *Inorg. Chem.* **2000**, *39*, 2314. (b) Deubel, D. V.; Sundermeyer, J.; Frenking, G. *J. Am. Chem. Soc.* **2000**, *122*, 10101. (c) Deubel, D. V.; Frenking, G.; Senn, H. M.; Sundermeyer, J. *Chem. Commun.* **2000**, 2469. (d) Deubel, D. V.; Sundermeyer, J.; Frenking, G. *Org. Lett.* **2001**, *3*, 329. (e) Deubel, D. V.; Sundermeyer, J.; Frenking, G. *Eur. J. Inorg. Chem.* **2001**, I00427, in press.

(9) Jørgensen, K. A.; Hoffmann, R. *Acta Chem. Scand. B* **1986**, *40*, 411.

(10) (a) Purcell, K. F. *J. Organomet. Chem.* **1983**, *252*, 181. (b) Purcell, K. F. *Organometallics* **1985**, *4*, 509.

(11) Ti-catalyzed olefin epoxidation has also theoretically been studied; for example, see: (a) Wu, Y. D.; Lai, D. K. W. *J. Am. Chem. Soc.* **1995**, *117*, 11327. (b) Wu, Y. D.; Lai, D. K. W. *J. Org. Chem.* **1995**, *60*, 673. (c) Karlsen, E.; Schoffel, K. *Catal. Today* **1996**, *32*, 107. (d) Tantanak, D.; Vincent, M. A.; Hillier, I. H. *Chem. Commun.* **1998**, 1031. (e) Sinclair, P. E., Carlow, C. R. A. *J. Phys. Chem. B* **1999**, *103*, 1084. (f) Yudanov, I. V.; Gisdakis, P.; Di Valentin, C.; Rösch, N. *Eur. J. Inorg. Chem.* **1999**, 2135.

(12) Sundermeyer, J. *Angew. Chem.* **1993**, *105*, 1195; *Angew. Chem., Int. Ed. Engl.* **1993**, *32*, 1144.

(13) Sharpless, K. B.; Townsend, J. M.; Williams, D. R. *J. Am. Chem. Soc.* **1972**, *94*, 295.

(14) Chemical reactions can be classified with respect to the topology of the transition state: (i) Reactions with a linear TS topology such as S_N2 reactions, (ii) pericyclic reactions, for instance Diels−Alder reactions, and (iii) reactions with a coarctate TS topology such as olefin epoxidation with peroxy acids (ref 15) or dioxiranes (ref 16). Reactions of the latter class proceed by breaking and making two bonds at one or more atoms at a time. For details, see: (a) Herges, R. *Angew. Chem.* **1994**, *106*, 261. (b) Herges, R. *J. Chem. Inf. Comput. Sci.* **1994**, *34*, 91.

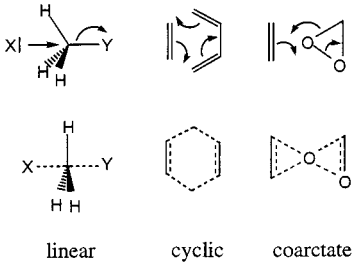

(15) (a) Plesnicar, B.; Tasevski, M.; Azman, A. *J. Am. Chem. Soc.* **1978**, *100*, 743. (b) Bach, R. D.; Owensby, A. L.; Gonzalez C.; Schlegel, H. B. *J. Am. Chem. Soc.* **1991**, *113*, 2338. (c) Yamabe, S.; Kondou C.; Minato, T. *J. Org. Chem.* **1996**, *61*, 616. (d) Singleton, D. A.; Merrigan, S. R.; Liu, J.; Houk, K. N. *J. Am. Chem. Soc.* **1997**, *119*, 3385. (e) Bach, R. D.; Canepa, C.; Winter, J. E.; Blanchette, P. E. *J. Org. Chem.* **1997**, *62*, 5191. (f) Bach, R. D.; Glukhovtsev, M. N.; Gonzalez, C.; Marquez, M.; Estevez, C. M.; Baboul, A. G.; Schlegel, H. B. *J. Phys. Chem.* **1997**, *101*, 6092. (g) Bach, R. D.; Estévez, C. M.; Winter, J. E.; Glukhovtsev, M. N. *J. Am. Chem. Soc.* **1998**, *120*, 680. (h) Bach, R. D.; Glukhovtsev, M. N.; Canepa, C. *J. Am. Chem. Soc.* **1998**, *120*, 775. (i) Bach, R. D.; Glukhovtsev, M. N.; Gonzalez, C. *J. Am. Chem. Soc.* **1998**, *120*, 9902. (j) Freccero, M.; Gandolfi, R.; Sarzi-Amadè, M.; Rastelli, A. *J. Org. Chem.* **1999**, *64*, 3853. (k) Marchand, A. P.; Ganguly, B.; Shukla, R.; Krishnudu, K.; Kumar, V. S.; Watson, W. H.; Bodige, S. G. *Tetrahedron* **1999**, *55*, 8313. (l) Freccero, M.; Gandolfi, R.; Sarzi-Amadè, M. *Tetrahedron* **1999**, *55*, 11309. (m) Freccero, M.; Gandolfi, R.; Sarzi-Amadè, M.; Rastelli, A. *J. Org. Chem.* **2000**, *65*, 2030. (n) Chekroun, A.; Jarid, A.; Benharref, A.; Boutalib, A. *J. Org. Chem.* **2000**, *65*, 4431. (o) Adam, W.; Bach, R. D.; Dmitrenko, O.; Saha-Möller, C. R. *J. Org. Chem.* **2000**, *65*, 6715. (p) Gisdakis, P.; Rösch, N. *Eur. J. Org. Chem.* **2001**, 719. (q) Deubel, D. V. *J. Org. Chem.* **2001**, *66*, JO010127M, accepted.

(16) (a) Bach, R. D.; Owensby, A. L.; Andres, J. L.; Schlegel, H. B. *J. Am. Chem. Soc.* **1991**, *113*, 7031. (b) Bach, R. D.; Andres, J. L.; Owensby, A. L.; Schlegel, H. B.; McDouall, J. J. W. *J. Am. Chem. Soc.* **1992**, *114*, 7207. (c) Houk, K. N.; Liu, J.; DeMello, N. C.; Condroski, K. R. *J. Am. Chem. Soc.* **1997**, *119*, 10147. (d) Jenson, C.; Liu, J.; Houk, K. N.; Jørgensen, W. L. *J. Am. Chem. Soc.* **1997**, *119*, 12982. (e) Miaskiewicz, K.; Smith, D. A. *J. Am. Chem. Soc.* **1998**, *120*, 1872. (f) Liu, J.; Houk, K. N.; Dinoi, A.; Fusco, C.; Curci, R. *J. Org. Chem.* **1998**, *63*, 8565. (g) Baboul, A. G.; Schlegel, H. B.; Glukhovtsev, M. N.; Bach, R. D. *J. Comput. Chem.* **1998**, *12*, 1353. (h) Freccero, M.; Gandolfi, R.; Sarzi-Amadè, M.; Rastelli, A. *Tetrahedron* **1998**, *54*, 12323. (i) Selcuki, C.; Aviyente, V. *J. Mol. Structure (THEOCHEM)* **1999**, *492*, 165. (j) Armstrong, A.; Washington, I.; Houk, K. N. *J. Am. Chem. Soc.* **2000**, *122*, 6297.

(17) Hay, P. J.; Wadt, W. R. *J. Chem. Phys.* **1985**, *82*, 299.

(18) (a) Ziegler, T.; Rauk, A. *Theor. Chim. Acta* **1977**, *46*, 1. (b) Ziegler, T.; Rauk, A. *Inorg. Chem.* **1979**, *18*, 1558. (c) Ziegler, T.; Rauk, A. *Inorg. Chem.* **1979**, *18*, 1755.

(19) For recent examples, see: (a) Fonseca Guerra, C.; Bickelhaupt, F. M.; Snijders, J. G.; Baerends, E. J. *J. Am. Chem. Soc.* **2000**, *122*, 4117. (b) Diefenbach, A.; Bickelhaupt, F. M.; Frenking, G. *J. Am. Chem. Soc.* **2000**, *122*, 6449. (c) Uddin, J.; Frenking, G. *J. Am. Chem. Soc.* **2001**, *123*, 1683.

(20) Becke, A. D. *Phys. Rev. A* **1988**, *38*, 3098.

(21) Perdew, J. P. *Phys. Rev. B* **1986**, *33*, 8822.

(22) Snijders, J. G.; Baerends, E. J.; Vernooijs, P. *At. Data Nucl. Tables* **1982**, *26*, 483.

(23) Baerends, E. J.; Ellis, D. E.; Ros, P. *Chem. Phys.* **1973**, *2*, 41.

(24) Krijn, J. G.; Baerends, E. J. *Fit Functions in the HFS-Method*; Internal Report (in Dutch); Vrije Universiteit Amsterdam: The Netherlands, 1984.

(25) Deubel, D. V.; Schlecht, S.; Frenking, G. *J. Am. Chem. Soc.* **2001**, *123*, JA003733, under revision.

(26) (a) Fonseca Guerra, C.; Snijders, J. G.; Te Felde, G.; Baerends, E. J. *Theor. Chem. Acc.* **1988**, *99*, 391. (b) Bickelhaupt, F. M.; Baerends, E. J. *Reviews in Computational Chemistry*; Lipkowitz, K. B., Boyd, D. B., Eds.; VCH: New York, 2000; Vol. 15, p 1.

(27) Becke, A. D. *J. Chem. Phys.* **1993**, *98*, 5648.

(28) Frenking, G.; Antes, I.; Böhme, M.; Dapprich, S.; Ehlers, A. W.; Jonas, V.; Neuhaus, A.; Otto, M.; Stegmann, R.; Veldkamp, A.; Vyboishchikov, S. F. *Reviews in Computational Chemistry*; Lipkowitz, K. B., Boyd, D. B., Eds.; VCH: New York, 1996; Vol. 8, p 63.

(29) Deubel, D. V.; Frenking, G. *J. Am. Chem. Soc.* **1999**, *121*, 2021.

(30) (a) Binkley, J. S.; Pople, J. A.; Hehre, W. J. *J. Am. Chem. Soc.* **1980**, *102*, 939. (b) Hehre, W. J.; Ditchfield, R.; Pople, J. A. *J. Chem. Phys.* **1972**, *56*, 2257.

(31) Ehlers, A. W.; Böhme, M.; Dapprich, S.; Gobbi, A.; Höllwarth, A.; Jonas, V.; Köhler, K. F.; Stegmann, R.; Veldkamp A.; Frenking, G. *Chem. Phys. Lett.* **1993**, *208*, 111.

(32) Clark, T.; Chandrasekhar, J.; Spitznagel, G. W.; Schleyer, P. v. R. *J. Comput. Chem.* **1983**, *4*, 294.

(33) Fukui, K. *Acc. Chem. Res.* **1981**, *14*, 363.

(34) Frisch, M. J.; Trucks, G. W.; Schlegel, H. B.; Scuseria, G. E.; Robb, M. A.; Cheeseman, J. R.; Zakrzewski, V. G.; Montgomery, J. A., Jr.; Stratmann, R. E.; Burant, J. C.; Dapprich, S.; Millam, J. M.; Daniels, A. D.; Kudin, K. N.; Strain, M. C.; Farkas, O.; Tomasi, J.; Barone, V.; Cossi, M.; Cammi, R.; Mennucci, B.; Pomelli, C.; Adamo, C.; Clifford, S.; Ochterski, J.; Petersson, G. A.; Ayala, P. Y.; Cui, Q.; Morokuma, K.; Malick, D. K.; Rabuck, A. D.; Raghavachari, K.; Foresman, J. B.; Cioslowski, J.; Ortiz, J. V.; Stefanov, B. B.; Liu, G.; Liashenko, A.; Piskorz, P.; Komaromi, I.; Gomperts, R.; Martin, R. L.; Fox, D. J.; Keith, T.; Al-Laham, M. A.; Peng, C. Y.; Nanayakkara, A.; Gonzalez, C.; Challacombe, M.; Gill, P. M. W.; Johnson, B. G.; Chen, W.; Wong, M. W.; Andres, J. L.; Head-Gordon, M.; Replogle, E. S.; Pople, J. A. *Gaussian 98*, revision A.6; Gaussian, Inc.: Pittsburgh, PA, 1998.

(35) (a) Pitzer, K. S. *Acc. Chem. Res.* **1979**, *12*, 271. (b) Pyykkö, P.; Desclaux, J. P. *Acc. Chem. Res.* **1979**, *12*, 279. (c) Christiansen, P. A.; Ermler, W. C.; Pitzer, K. S. *Annu. Rev. Phys. Chem.* **1985**, *36*, 407. (d) Pyykkö, P. *Chem. Rev.* **1988**, *88*, 563. (e) Almlöf, J.; Gropen, O. In *Reviews in Computational Chemistry*; Lipkowitz, K. B., Boyd, D. B., Eds.; VCH: New York, 1996; Vol. 8, p 203. (f) Balasubramanian, K. *Relativistic Effects in Chemistry*; Wiley: New York, 1997. (g) Schwerdtfeger P. *Relativistic Effects in Chemistry*; Lecture, University of Marburg, Germany, 1998.

(36) Dirac, P. A. M. *Proc. R. Soc. London* **1928**, *117*, 610.

(37) We have chosen a definition of the Dirac equation with

$$\beta = \begin{pmatrix} 0 & 0 \\ 0 & -2 \end{pmatrix} \otimes \begin{pmatrix} 1 & 0 \\ 0 & 1 \end{pmatrix}$$

instead of

$$\beta = \begin{pmatrix} 1 & 0 \\ 0 & -1 \end{pmatrix} \otimes \begin{pmatrix} 1 & 0 \\ 0 & 1 \end{pmatrix}$$

to align the nonrelativistic and relativistic energy scales.

(38) (a) Snijders, J. G.; Baerends, E. J. *Mol. Phys.* **1979**, *36*, 1789. (b) Snijders, J. G.; Baerends, E. J.; Ros, P. *Mol. Phys.* **1979**, *38*, 1909.

(39) (a) Chang, C.; Pelissier, M.; Durand, P. *Phys. Scr.* **1986**, *34*, 394. (b) Heully, J.-L.; Lindgren, I.; Lindroth, E.; Lundquist, S.; Martensson-Pendrill, A. M. *J. Phys. B* **1986**, *19*, 2799. (c) Van Lenthe, E.; Baerends, E. J.; Snijders, J. G. *J. Chem. Phys.* **1993**, *99*, 4597. (d) Van Lenthe, E.; Baerends, E. J.; Snijders, J. G. *J. Chem. Phys.* **1994**, *101*, 9783. (e) Van Lenthe, E.; Snijders, J. G.; Baerends, E. J. *J. Chem. Phys.* **1996**, *105*, 6505. (f) Van Lenthe, E.; Van Leeuwen, R.; Baerends, E. J.; Snijders, J. G. *Int. J. Quantum Chem.* **1996**, *57*, 281. (g) Van Lenthe, E.; Ehlers, A. E.; Baerends, E. J. *J. Chem. Phys.* **1999**, *110*, 8943.

(40) (a) Bersuker, I. B.; Budnikov, S. S.; Leizerov, B. A. *Int. J. Quantum Chem.* **1972**, *6*, 849. (b) Cowan, R. D.; Griffin, D. C. *J. Opt. Soc. Am.* **1976**, *66*, 1010. (c) Ziegler, T.; Tschinke, V.; Baerends, E. J.; Snijders, J. G.; Ravenek, W. *J. Phys. Chem.* **1989**, *93*, 3050.

(41) The transition states show a significant anomeric effect, which was pointed out in our previous studies (ref 8ab). In the TS, the phosphorus−oxygen bond (P−O6) has a synperiplanar orientation to the active metalladioxirane moiety (M, O2, O3; see Figure 1) because the lone pair of O6 with an antiperiplanar orientation to the active metalladioxirane moiety supports the cleavage of the Mo−O3 bond.

(42) There is no experimental activation energy available because the kinetic data presented in the pioneering work (ref 2b) were interpreted in favor of the wrong mechanism. BP86 activation barriers for the epoxidation of olefins with organic peracids (ref 15) are several kcal/mol lower than B3LYP values, which in turn underestimate experimental activation energies. In the present work, we employ the BP86 functional because both the fragment-based energy-decomposition scheme and BP86 are implemented in the ADF package while the hybrid functional is not.

(43) (a) Bell, R. P. *Proc. R. Soc. London, Ser. A* **1936**, *154*, 414. (b) Evans, M. G.; Polanyi, M. *J. Chem. Soc., Faraday Trans.* **1936**, *32*, 1340.

(44) Hammond, G. S. *J. Am. Chem. Soc.* **1955**, *77*, 334.

(45) The relation among the extent of reaction, the extent of asymmetry, and the electronic character at the TS for the epoxidation of various α olefins with peroxyformic acid and dioxirane was recently studied and the effects on reactivity were pointed out; for details, see ref 15q.

(46) The attack of the σ^*-(O−O) Orbital of electrophilic oxidants was postulated by Edwards: (a) Edwards, J. O. In *Peroxide Reaction Mechanisms*; Edwards, J. O., Ed.; Interscience: New York, 1962; p. 67. (b) Curci, R.; Edwards, J. O. In *Catalytic Oxidations with Hydrogen Peroxide as Oxidant*; Strukul, G., Ed.; Kluwer: Dordrecht, 1992; p. 45.

(47) The geometries of TS− and TS+ were calculated by adding −0.1 and 0.1, respectively, of the eigenvector that corresponds to the negative eigenvalue of the force-constants matrix to the coordinates of the stationary point.

(48) (a) Ziegler, T.; Snijders, J. G.; Baerends, E. J. *Chem. Phys. Lett.* **1980**, *75*, 1. (b) Snijders, J. G.; Pyykkö, P. *Chem. Phys. Lett.* **1980**, *75*, 5. (c) Pyykkö, P.; Snijders, J. G.; Baerends, E. J. *Chem. Phys. Lett.* **1981**, *83*, 432. (d) Ziegler, T.; Snijders, J. G.; Baerends, E. J. *J. Chem. Phys.* **1981**, *74*, 1271.